Nanoscale

PAPER

View Article Online
View Journal | View Issue

Cite this: *Nanoscale*, 2018, **10**, 15387

$Ti_2C_3T_x$ nanosheets as photothermal agents for near-infrared responsive hydrogels†

Changyu Yang, Danyun Xu, WenChao Peng, Yang Li, Guoliang Zhang, Fengbao Zhang and Xiaobin Fan *

Received 2nd July 2018,
Accepted 18th July 2018

DOI: 10.1039/c8nr05301d

rsc.li/nanoscale

Poly(*N*-isopropylacrylamide) (PNIPAM) is broadly applicable in many fields due to its temperature-induced phase transition property. Herein, a facile method to incorporate exfoliated $Ti_2C_3T_x$ nanosheets in the PNIPAM network is reported. Due to compatibility, stability and photothermal properties of the incorporated $Ti_2C_3T_x$ nanosheets, the obtained MXene/PNIPAM composite hydrogel shows excellent photothermal properties, expanding the pure thermal-responsive property of the PNIPAM hydrogel. Based on the smart composite hydrogel, remote light-control of the microfluidic pipeline is also demonstrated.

Introduction

As an important type of intelligent material, multifunctional hydrogel has received considerable attention due to external stimuli (temperature, light, pH, *etc.*), high biocompatibility and water-rich in nature.[1–3] Such properties make these materials broadly applicable in the fields of drug delivery, tissue engineering, microdevices, *etc.*[4–6] Among the diverse hydrogels, poly(*N*-isopropylacrylamide) (PNIPAM) is a typical type of temperature-sensitive hydrogel, which has been widely studied.[7–9] PNIPAM exhibits temperature-induced reversible phase transition (volume change) in an aqueous solution at a lower critical solution temperature (LCST) due to the presence of both hydrophilic amide groups and hydrophobic isopropyl groups in its side chains.[10] However, there have been limited studies on the remote phase transition of PNIPAM due to its pure thermal-responsive property.

As we know, many photothermal materials can generate heat when exposed to near-infrared (NIR) irradiation. Thereby, we can incorporate photothermal materials in PNIPAM hydrogels to fabricate a composite hydrogel, which can generate heat upon light stimulation, actuating the temperature-sensitive hydrogels remotely. Two-dimensional nanomaterials, which usually have high infrared absorption properties, are promising candidates as photothermal agents. For example, graphene and its derivatives have shown excellent photothermal properties, and they are widely applied in photothermal therapy.[11] However, graphene and reduced graphene oxide (rGO) are both hydrophobic; thus, they require complex surface modification to incorporate PNIPAM, whereas the photothermal efficacy of the hydrophilic graphene oxide (GO) is still under debate.[12–14] In addition, transition metal dichalcogenides (TMDs), such as 1T phase molybdenum disulfide (MoS_2), have excellent hydrophilic and photothermal properties.[15] However, 1T phase MoS_2 is metastable and may gradually change to hydrophobic 2H phase with lower photothermal efficacy upon long-term NIR irradiation,[16] which restricts its effective application in fields such as microfluidic valves. Therefore, it is increasingly desirable and challenging to develop new photothermal agents with excellent compatibility, stability and photothermal properties.

$Ti_2C_3T_x$ (T_x stands for –OH, =O and –F functional groups), as a member of two-dimensional materials in the MXene family,[17] is generally produced by selective etching of Ti_2AlC_3 in acid fluoride-containing solutions.[18] In the etching process, Al elements are substituted with –OH, =O, or –F functional groups, resulting in typical hydrophilic nature.[19] $Ti_2C_3T_x$ also has excellent photothermal properties, which are equivalent to or even superior to those of other materials such as carbon-based materials, TMDs and gold-based nanostructures.[20] The photothermal conversion efficiency of $Ti_2C_3T_x$ nanosheets can reach 30.6% upon NIR laser irradiation (808 nm).[21] This value is higher than those of Au nanorods (21%),[22] $Cu_{2-x}Se$ nanosheets (22%)[23,24] and Cu_9S_5 nanosheets (25.7%).[25] Furthermore, unlike metastable 1T-MoS_2, which may undergo 1T to 2H phase change upon long-term NIR irradiation, $Ti_2C_3T_x$ nanosheets show much better thermal stability. Only high-temperature annealing (*e.g.*, 500 °C) can lead to the reduction of the OH terminations on the $Ti_2C_3T_x$ nanosheets.[26] Herein, we have found that $Ti_2C_3T_x$ can be used as an ideal photothermal agent to fabricate PNIPAM-based composite hydrogels with excellent NIR-responsive properties

School of Chemical Engineering & Technology, State Key Laboratory of Chemical Engineering, Collaborative Innovation Center of Chemical Science and Engineering, Tianjin University, Tianjin, 300072, China. E-mail: xiaobinfan@tju.edu.cn

†Electronic supplementary information (ESI) available. See DOI: 10.1039/c8nr05301d

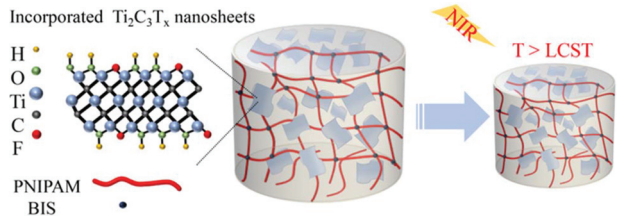

Scheme 1 Remote light-controlled MXene/PNIPAM composite hydrogels.

(Scheme 1); their application in remote light-control of the microfluidic pipeline is also demonstrated.

Results and discussion

The morphology of the obtained $Ti_2C_3T_x$ nanosheets was characterized by transmission electron microscopy (TEM), and the results showed a two-dimensional structure with lateral sizes of 0.5–1 μm (Fig. 1a and Fig. S1†). The high transparency of these $Ti_2C_3T_x$ nanosheets indicated their single-layer nature, which was further supported by the results of atomic force microscopy (AFM). As shown in Fig. 1b, by line scanning across the sheets, the apparent AFM thickness of these $Ti_2C_3T_x$ nanosheets was measured to be approximately 2 nm, and the results were in agreement with previously reported observations.[20] It should be mentioned that the measured thickness of the monolayer $Ti_2C_3T_x$ sheet was larger than the theoretical value (~0.98 nm) calculated by the density functional theory (DFT).[27] Similar to that observed for other 2D materials, the increased thickness is probably due to intrinsic ripples[28,29] and the unavoidable trapping of solvents under the sheet surfaces.[30,31]

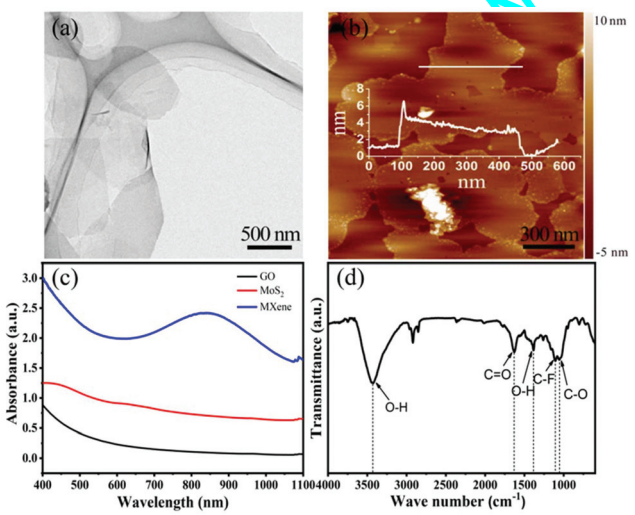

Fig. 1 (a) Representative bright-field TEM and (b) AFM image of exfoliated $Ti_2C_3T_x$ sheets (please see the ESI† for the lateral size and height distribution details); (c) UV-vis-NIR absorbance spectra of the same concentration (0.1 mg mL^{-1}) of $Ti_2C_3T_x$, MoS_2, and GO in aqueous solution. (d) FTIR spectra of $Ti_2C_3T_x$ nanosheets.

Apart from the monolayer nature, we found that the exfoliated $Ti_2C_3T_x$ nanosheets showed desirable high absorbance in the near-infrared (NIR) region. Fig. 1c presents the UV-vis-NIR absorption spectra (400–1100 nm) of $Ti_2C_3T_x$, 1T-MoS_2 and GO dispersion with the same mass concentration of 0.1 mg mL^{-1}. We can see that GO and MoS_2 showed a broad absorption spectrum from 400 to 1100 nm without any clear absorption peak, whereas $Ti_2C_3T_x$ displayed a clear and much higher absorption peak at around 850 nm. The UV-vis-NIR absorption of the composite hydrogel (with 0.1 mg mL^{-1} $Ti_2C_3T_x$ nanosheets) was measured, as shown in Fig. S3.† No characteristic absorption of MXene could be found, which was due to its limited content in the composite. Moreover, the mass extinction coefficient of $Ti_2C_3T_x$ at 808 nm was calculated according to the Lambert–Beer law to be 17.35 L g^{-1} cm^{-1} (please see Fig. S4† for more details). Fig. 3d shows the FTIR spectra of $Ti_2C_3T_x$ nanosheets. The stretching vibrations at around 3400 cm^{-1}, 1645 cm^{-1}, 1050 cm^{-1} and 1090 cm^{-1} were assigned to O–H, C=O, C–O and C–F bonds, respectively.[32,33] The observed functional groups demonstrated high hydrophilic property of the $Ti_2C_3T_x$ nanosheets. The strong absorption of $Ti_2C_3T_x$ in the NIR region combined with its hydrophilic nature demonstrated its great potential as a new type of photothermal agent for composite hydrogels. Therefore, the exfoliated $Ti_2C_3T_x$ nanosheets were homogeneously incorporated in PNIPAM by direct polymerization of *N*-isopropylacrylamide monomer (NIPAM) in the presence of MXene.

As shown in the inserted optical images of Fig. 2a and b, there are dramatic differences in color between the composite hydrogels and pure PNIPAM. The composite hydrogel, instead of remaining transparent, became homogeneous and black after incorporation of $Ti_2C_3T_x$. To better understand the microstructure and distribution, we analyzed the composite hydrogels (with 1.0 mg mL^{-1} $Ti_2C_3T_x$) using a scanning electron microscope (SEM) and the X-ray energy dispersion spectrum (EDS). Similar to pure hydrogels (Fig. 2a), the composite hydrogels retained their interconnected network and macroporous structure without substantial changes after incorporation (Fig. 2b), indicating that the $Ti_2C_3T_x$ nanosheets did not influence the microstructure of the PNIPAM matrix. Moreover, the EDS spectrum of the composite hydrogel (Fig. 2c–e) demonstrates the coexistence of C, N and Ti despite the weaker signal of the Ti element, which was due to low loading of $Ti_2C_3T_x$. The successful incorporation of $Ti_2C_3T_x$ was further confirmed by Raman spectroscopy (Fig. 2f). The characteristic Raman peaks of $Ti_2C_3T_x$ could be easily detected for the MXene/PNIPAM composite hydrogels. Specifically, the modes at 206 (ω_2) and 717 cm^{-1} (ω_3) are the A_{1g} symmetry out-of-plane vibrations of Ti and C atoms, respectively, whereas the modes at 280 (ω_5), 368 (ω_5), and 626 cm^{-1} (ω_4) are the E_g group vibrations including the in-plane (shear) modes of Ti, C, and surface functional group atoms.[34,35] Compared with the result for pure $Ti_2C_3T_x$, there was no clear peak shift for the composite hydrogels, indicating that no or few defects were introduced into the $Ti_2C_3T_x$ sheet during incorporation.

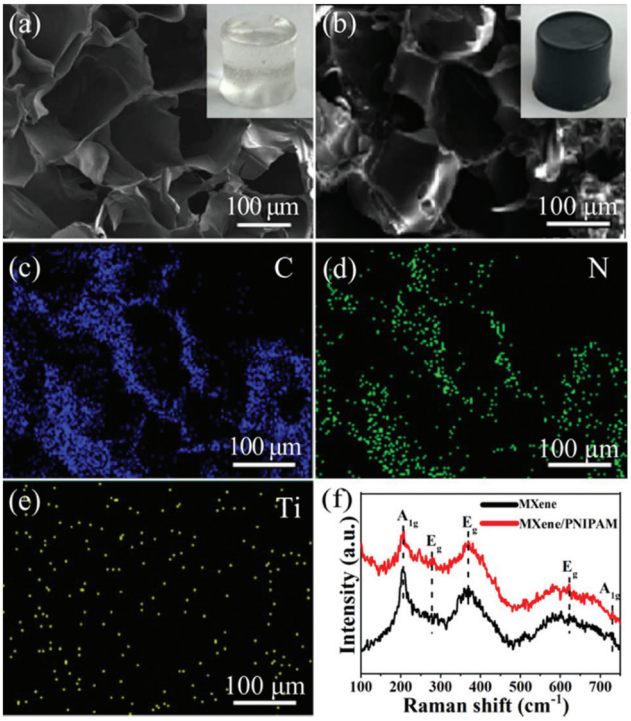

Fig. 2 (a) SEM image of the freeze-dried pure PNIPAM hydrogel (b) SEM image of the freeze-dried MXene/PNIPAM composite hydrogel and its associated EDS element mapping of (c) C, (d) N, (e) Ti. (f) Raman spectra of MXene/PNIPAM composite hydrogel (with 1.0 mg mL^{-1} $Ti_2C_3T_x$) compared with the pristine $Ti_2C_3T_x$, showing that no peaks shift after incorporation. Inset: Digital photographs of pure PNIPAM (a) and the MXene/PNIPAM composite hydrogel with 1.0 mg mL^{-1} $Ti_2C_3T_x$ (b).

According to differential scanning calorimetry (DSC), in which the endothermic peak in the DSC curves shows the critical volume phase transition temperature (VPTT), the VPTT value of pure PNIPAM hydrogel is around 30 °C, whereas the VPTT value of the composite hydrogels increases gradually as the amount of $Ti_2C_3T_x$ increases (Fig. 3a). This result can be explained by the hydrophilic nature of the incorporated $Ti_2C_3T_x$. It is known that LCST of PNIPAM-based hydrogels can be modulated with sudden alterations of hydrophilic/hydrophobic side groups.[10] Generally, LCST increases with the incorporation of hydrophilic copolymers[36,37] and decreases with hydrophobic copolymers.[36,38] To evaluate the effect of temperature on the volume change of hydrogels, the swelling ratios of hydrogels under different temperatures are measured (Fig. 3b). From the swelling ratio curves, we can see that these hydrogels show sudden volume contraction at around 30 °C during the volume phase transition, which is in agreement with the DSC curves. In addition, the hydrogels show high temperature sensitivity and swelling ratio. However, the composite hydrogels with higher $Ti_2C_3T_x$ contents (*e.g.*, 1.5 mg mL^{-1}) exhibit more clear reduction in swelling and deswelling capacities when the temperature is above LCST. This phenomenon can be due to the increased interaction between PNIPAM and excessive $Ti_2C_3T_x$ nanosheets, which may hinder the coil-to-globule transition of PNIPAM. Furthermore, compression tests have been carried out to measure the modulus and strength at break. The detailed analyses obtained from the typical stress–strain curves are presented in Fig. S5.† In particular, the pure PNIPAM hydrogel exhibits almost 0.13 MPa at 64% strain, and the Young's modulus is 8.66 kPa. In comparison, the composite PNIPAM hydrogel (with 1.0 mg ml^{-1} $Ti_2C_3T_x$) exhibits almost 0.17 MPa at 64% strain, and the Young's modulus is 9.97 kPa. It has been reported that the entanglement between polymer chains and networks inside a hydrogel can significantly increase the mechanical properties of the hydrogel.[39] Therefore, the composite hydrogels become more elastic and stretchable than pure PNIPAM.

To further verify photothermal properties, 0.5 cm^3 MXene/PNIPAM composite hydrogels (with different concentrations of $Ti_2C_3T_x$) and pure hydrogel were placed in 0.5 ml of water. The hydrogels were then exposed to an 808 nm NIR laser with a power of 0.8 W. As presented in Fig. 3c, the temperature of water with the incorporated composite hydrogels (1 mg mL^{-1} $Ti_2C_3T_x$) rose by over 20 °C in 5 minutes. In comparison, there was nearly no increase in temperature for the counterpart with the pure hydrogel under the same irradiation condition. These results further confirmed that $Ti_2C_3T_x$ is the main light-to-heat conversion material. Similar to previously reported results with other photothermal agents,[12,40] the temperature increase was not only associated with the time of irradiation but also with the mass concentration of $Ti_2C_3T_x$. Hence, we may consider the mass concentration of $Ti_2C_3T_x$ for controlling the speed of heating and temperature of the system. However, we found that minimal change can be observed after 3 minutes of irradiation when the concentration of $Ti_2C_3T_x$ reached 1 mg mL^{-1}. This phenomenon can be explained by the logarithmic absorbance dependence of the fraction of incident radiation[41] and rapid heat loss at relatively high temperatures.[42]

The stability and reusability of MXene/PNIPAM composite under laser irradiation were also tested to evaluate the potential of MXenes as a photothermal agent in hydrogels. As shown in Fig. 3d, $Ti_2C_3T_x$ remained as a photothermal heater even after 24 cycles of NIR irradiation (each cycle was continued for 2.5 minutes of NIR irradiation), showing nearly unchanged temperature increase in each cycle. Furthermore, the photothermal phase transition of the MXene/PNIPAM composite hydrogel could be easily observed under NIR laser irradiation (808 nm) (Fig. 3e). When the NIR laser was turned on, the composite hydrogel showed significant volume shrinkage. It is noteworthy that the collapsed hydrogel could readily return to its original state when the laser was turned off. For all thermal-responsive hydrogels, the time required for the hydrogel to return to its original state depends on the cooling rate, which is closely related to the cooling methods, the environmental temperature, the thermal conductivity of the liquid and the pipeline. In our case, the hydrogel cooled naturally, and ~5 minutes were required for the hydrogel to recover its original size. These phenomena indicate that the phase change process is completely reversible.

To test whether the composite hydrogel can be applied to microfluidic devices, a simple MXene/PNIPAM hydrogel-based

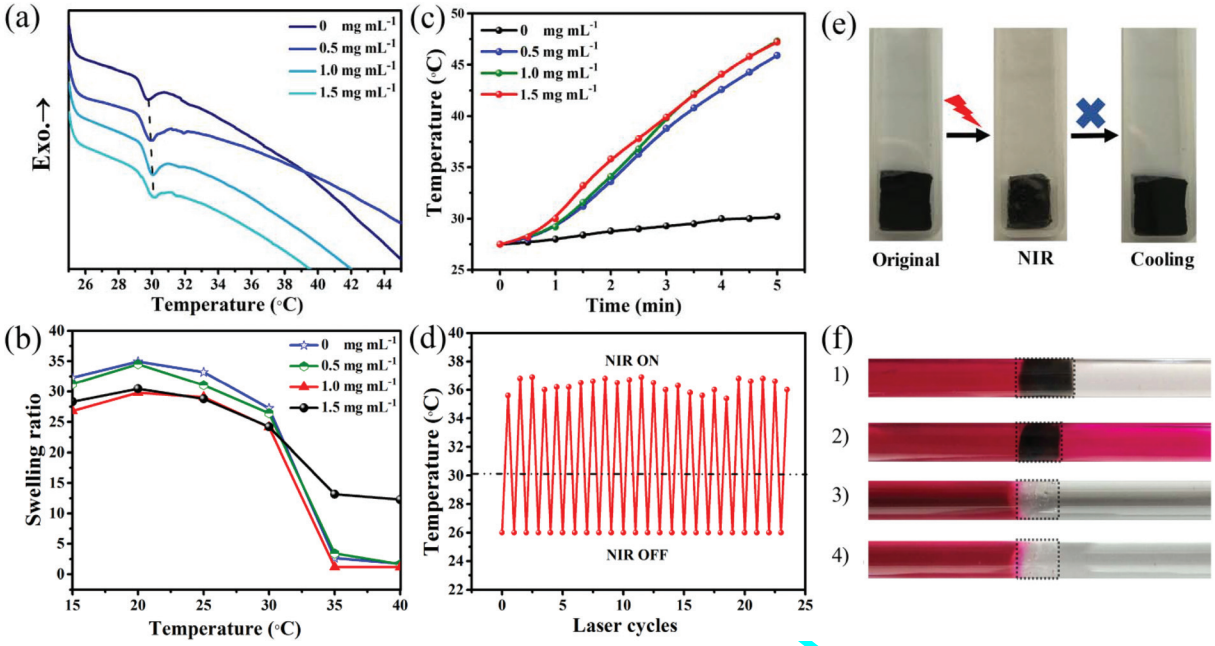

Fig. 3 (a) DSC analysis of pure hydrogel and MXene/PNIPAM composite hydrogels with 0.5 mg mL^{-1}, 1.0 mg mL^{-1}, 1.5 mg mL^{-1} of $Ti_2C_3T_x$ at a temperature ramp of 1 °C min^{-1} in N_2 from 25 to 45 °C. (b) Swelling ratio dependence on temperature for pure PNIPAM and MXene/PNIPAM composite hydrogels. (c) The temperature of 0.5 ml water with the pure hydrogel and MXene/PNIPAM composite hydrogels. (d) The temperature changes of the MXene/PNIPAM composite hydrogel (with 1 mg mL^{-1} $Ti_2C_3T_x$) as a function of heating–cooling cycles. (e) Photograph of the volume change of the MXene/PNIPAM composite hydrogel (with 1 mg mL^{-1} $Ti_2C_3T_x$) before and after NIR laser irritation. (f) Liquid microvalves fabricated by the MXene/PNIPAM composite hydrogel (1, 2) and pure PNIPAM hydrogel (3, 4). The photographs show the microvalves before (1, 3) and after (2, 4) exposure to NIR irradiation (808 nm, 0.8 W) for 1 min. The solutions injected in the microfluidic pipelines (5.0 mm in inner diameter) are red rhodamine solution and water, respectively.

microvalve was constructed in the microfluidic pipelines, and the PNIPAM hydrogel was used for comparison. As shown in Fig. 3f, the composite hydrogel separated the red rhodamine B solution and transparent distilled water completely before NIR irradiation. Once the laser was switched on, the composite hydrogel shrank and allowed the fluidic flow of rhodamine B solution from left to right, resulting in the color change of the distilled water (more details are provided in the ESI Video 1†). In contrast, the pure PNIPAM hydrogel blocked the flow with or without laser irradiation. These results suggested that the MXene/PNIPAM composite hydrogel has potential application in remote light-controlled microfluidic devices.

Conclusions

In conclusion, we found that MXene ($Ti_2C_3T_x$) can be readily incorporated in PNIPAM, and the novel MXene/PNIPAM composite hydrogel was prepared. The obtained composite hydrogel showed excellent photothermal properties, resulting in a clear trend of temperature increase under NIR laser irradiation. In addition, the reversible volume phase transition could be remotely controlled by NIR. To evaluate the potential of this new hydrogel, an MXene/PNIPAM-based microvalve was fabricated, and its application in the remote light-control of microfluidic pipelines was demonstrated. We believe that this strategy can be easily used to prepare a variety of MXene/PNIPAM hydrogels, and their potential applications in biomedicine, drug delivery and catalysis should be explored.

Experimental

Materials and methods

We used Ti_3AlC_2 (starting material) (98%, Forsman), hydrofluoric acid (HF, 40%, Aladdin), tetramethyl ammonium hydroxide (TMAOH, 25%, TGI), *N*-isopropylacrylamide (NIPAM, 98%, TGI), *N*,*N*′-methylenebis(acrylamide) cross-linker (BIS, 99%, Aladdin), *N*,*N*,*N*′,*N*′-tetramethylethylenediamine (TMEDA, 98%, TGI), ammonium peroxodisulfate (APS, 20%, Aladdin), and rhodamine B (98%, Guang Fu).

Synthetic procedures

Synthesis of exfoliated $Ti_2C_3T_x$ nanosheets. Two g Ti_3AlC_2 powder and 20 ml 20 wt% HF solution were mixed and stirred for 30 min to etch Al. After etching, the suspension was centrifuged at 12 000 rpm for 10 min to remove excess HF and etched Al. To obtain single-layer thin nanosheets, 50 ml of 25 wt% TMAOH solution was added to the etched samples and shaken for 24 h on a rotary shaker at room temperature.

Subsequent centrifugation at 12 000 rpm was performed to remove excess TMAOH. The resulting suspension was centrifuged at 3500 rpm for 10 min to remove undelaminated powder and thick flakes.

Synthesis of MXene/PNIPAM nanocomposite hydrogels. Various amounts of $Ti_2C_3T_x$ powder (0, 0.5 mg mL^{-1}, 1 mg mL^{-1}, 1.5 mg mL^{-1}) were dispersed in 10 ml deionized water by ultrasonication with an ice water bath for 20 min. Then, 700 mg *N*-isopropylacrylamide monomer and 6 mg *N*,*N*′-methylenebis(acrylamide) cross-linker were added with stirring. The resulting solution was purged with pure argon for 10 min to remove any dissolved oxygen. After that, 10 μL *N*,*N*,*N*′,*N*′-tetramethylethylenediamine as a polymerization accelerator and 20 μL 20 wt% ammonium peroxodisulfate aqueous solution as an initiator were added successively. The polymerization was completed in a 20 ml glass bottle for 24 h at room temperature. The obtained hydrogels were washed with deionized water to remove any excess monomer and $Ti_2C_3T_x$. The pure hydrogels were synthesized in the same way but without $Ti_2C_3T_x$.

Fabrication of microfluidic valves. To verify the application performance of the hydrogel in the microfluidic pipeline, the cylindrical composite hydrogel and pure hydrogel were respectively inserted into a quartz tube 5.0 mm in inner diameter. Please note that the cylindrical composite hydrogel with a diameter larger than that of the pipeline was exposed to NIR irradiation first. Then, the shrunken hydrogel can be easily inserted into the pipeline. When cooled to a temperature lower than its LCST, the hydrogel expanded and blocked the fluid flow in the pipeline. Red rhodamine B solution and deionized water were injected into each side of the hydrogel in the quartz tube. When exposed to 808 nm laser irradiation (0.8 W) for ~1 min, the composite hydrogel shrank, resulting in the fluidic flow, and the color of the deionized water changed. In contrast, when the pure hydrogel was used, no flow was observed.

Characterization. Samples were characterized by transmission electron microscopy (TEM, JEM-2100F), at an acceleration voltage of 200 kV, Atomic force microscopy (AFM, CSPM 5000), UV–vis spectroscopy (Unico, UV-3802), scanning electron microscopy (SEM, Hitachi S-4800), energy-dispersive X-ray spectroscopy (EDX, FEI NOVA NanoSEM 430), and Raman spectroscopy (HORIBA Spectra, LabRam HR Evolution) with 633 nm laser excitation (10% laser power). Differential scanning calorimetry (DSC, Mettler-Toledo, Switzerland) was carried out under an N_2 atmosphere at a temperature ramp of 1.0 °C min^{-1} from 25 to 45 °C. To determine the swelling ratio (S_r) of hydrogels, all samples were immersed in water and equilibrated for 2 days at various temperatures. S_r was calculated *via* the following equation: $S_r = (W_w - W_d)/W_d$, where W_w is the weight of the wet state at swelling equilibrium, and W_d is the weight of the hydrogel in the dry state.

Conflicts of interest

There are no conflicts to declare.

Acknowledgements

This study is supported by the National Natural Science Funds (no. 21676198) and the Program of Introducing Talents of Discipline to Universities (no. B06006).

Notes and references

1 M. C. Koetting, J. T. Peters, S. D. Steichen and N. A. Peppas, *Mater. Sci. Eng., R*, 2015, **93**, 1–49.
2 S. Rittikulsittichai, A. G. Kolhatkar, S. Sarangi, M. A. Vorontsova, P. G. Vekilov, A. Brazdeikis and T. Randall Lee, *Nanoscale*, 2016, **8**, 11851–11861.
3 S. Naahidi, M. Jafari, M. Logan, Y. Wang, Y. Yuan, H. Bae, B. Dixon and P. Chen, *Biotechnol. Adv.*, 2017, **35**, 530–544.
4 J. Li and D. J. Mooney, *Nat. Rev. Mater.*, 2016, **1**, 16071.
5 H. Liu, C. Wang, C. Li, Y. Qin, Z. Wang, F. Yang, Z. Li and J. Wang, *RSC Adv.*, 2018, **8**, 7533–7549.
6 S. Lin, W. Wang, X. J. Ju, R. Xie and L. Y. Chu, *Lab Chip*, 2014, **14**, 2626–2634.
7 A. Halperin, M. Kröger and F. M. Winnik, *Angew. Chem., Int. Ed.*, 2015, **54**, 15342–15367.
8 C. Yao, Z. Liu, C. Yang, W. Wang, X.-J. Ju, R. Xie and L.-Y. Chu, *Adv. Funct. Mater.*, 2015, **25**, 2980–2991.
9 F. F. Sahle, M. Giulbudagian, J. Bergueiro, J. Lademann and M. Calderon, *Nanoscale*, 2017, **9**, 172–182.
10 T.-Y. Wu, A. B. Zrimsek, S. V. Bykov, R. S. Jakubek and S. A. Asher, *J. Phys. Chem. B*, 2018, **122**, 3008–3014.
11 Y.-W. Chen, Y.-L. Su, S.-H. Hu and S.-Y. Chen, *Adv. Drug Delivery Rev.*, 2016, **105**, 190–204.
12 C.-H. Zhu, Y. Lu, J. Peng, J.-F. Chen and S.-H. Yu, *Adv. Funct. Mater.*, 2012, **22**, 4017–4022.
13 J. Zhang, L. Song, Z. Zhang, N. Chen and L. Qu, *Small*, 2014, **10**, 2151–2164.
14 E. Zhang, T. Wang, W. Hong, W. Sun, X. Liu and Z. Tong, *J. Mater. Chem. A*, 2014, **2**, 15633–15639.
15 S. S. Chou, B. Kaehr, J. Kim, B. M. Foley, M. De, P. E. Hopkins, J. Huang, C. J. Brinker and V. P. Dravid, *Angew. Chem.*, 2013, **125**, 4254–4258.
16 X. Fan, P. Xu, D. Zhou, Y. Sun, Y. C. Li, M. A. T. Nguyen, M. Terrones and T. E. Mallouk, *Nano Lett.*, 2015, **15**, 5956–5960.
17 M. Naguib, V. N. Mochalin, M. W. Barsoum and Y. Gogotsi, *Adv. Mater.*, 2014, **26**, 992–1005.
18 M. Alhabeb, K. Maleski, B. Anasori, P. Lelyukh, L. Clark, S. Sin and Y. Gogotsi, *Chem. Mater.*, 2017, **29**, 7633–7644.
19 K. Maleski, V. N. Mochalin and Y. Gogotsi, *Chem. Mater.*, 2017, **29**, 1632–1640.
20 J. Xuan, Z. Wang, Y. Chen, D. Liang, L. Cheng, X. Yang, Z. Liu, R. Ma, T. Sasaki and F. Geng, *Angew. Chem.*, 2016, **128**, 14789–14794.
21 H. Lin, X. Wang, L. Yu, Y. Chen and J. Shi, *Nano Lett.*, 2017, **17**, 384–391.
22 Z. Jie, G. David and X. Younan, *Angew. Chem., Int. Ed.*, 2013, **52**, 4169–4173.

23 Q. Tian, F. Jiang, R. Zou, Q. Liu, Z. Chen, M. Zhu, S. Yang, J. Wang, J. Wang and J. Hu, *ACS Nano*, 2011, **5**, 9761–9771.
24 C. M. Hessel, V. P. Pattani, M. Rasch, M. G. Panthani, B. Koo, J. W. Tunnell and B. A. Korgel, *Nano Lett.*, 2011, **11**, 2560–2566.
25 L. Teng, W. Chao, G. Xing, G. Hua, C. Liang, S. Xiaoze, F. Liangzhu, S. Baoquan and L. Zhuang, *Adv. Mater.*, 2014, **26**, 3433–3440.
26 Y. Xie, M. Naguib, V. N. Mochalin, M. W. Barsoum, Y. Gogotsi, X. Yu, K.-W. Nam, X.-Q. Yang, A. I. Kolesnikov and P. R. C. Kent, *J. Am. Chem. Soc.*, 2014, **136**, 6385–6394.
27 X. Wang, X. Shen, Y. Gao, Z. Wang, R. Yu and L. Chen, *J. Am. Chem. Soc.*, 2015, **137**, 2715–2721.
28 R. J. T. Nicholl, H. J. Conley, N. V. Lavrik, I. Vlassiouk, Y. S. Puzyrev, V. P. Sreenivas, S. T. Pantelides and K. I. Bolotin, *Nat. Commun.*, 2015, **6**, 8789.
29 J. Brivio, D. T. L. Alexander and A. Kis, *Nano Lett.*, 2011, **11**, 5148–5153.
30 K. Xu, P. Cao and J. R. Heath, *Science*, 2010, **329**, 1188–1191.
31 O. Ochedowski, B. K. Bussmann and M. Schleberger, *Sci. Rep.*, 2014, **4**, 6003.
32 P. Yan, R. Zhang, J. Jia, C. Wu, A. Zhou, J. Xu and X. Zhang, *J. Power Sources*, 2015, **284**, 38–43.
33 Q. Xue, Z. Pei, Y. Huang, M. Zhu, Z. Tang, H. Li, Y. Huang, N. Li, H. Zhang and C. Zhi, *J. Mater. Chem. A*, 2017, **5**, 20818–20823.
34 M. Hu, Z. Li, T. Hu, S. Zhu, C. Zhang and X. Wang, *ACS Nano*, 2016, **10**, 11344–11350.
35 J. Yan, E. Ren Chang, K. Maleski, B. Hatter Christine, B. Anasori, P. Urbankowski, A. Sarycheva and Y. Gogotsi, *Adv. Funct. Mater.*, 2017, **27**, 1701264.
36 R. Yoshida, K. Sakai, T. Okano and Y. Sakurai, *J. Biomater. Sci., Polym. Ed.*, 1995, **6**, 585–598.
37 L. M. Geever, D. M. Devine, M. J. D. Nugent, J. E. Kennedy, J. G. Lyons and C. L. Higginbotham, *Eur. Polym. J.*, 2006, **42**, 69–80.
38 Y. H. Bae, T. Okano and S. W. Kim, *Pharm. Res.*, 1991, **8**, 531–537.
39 M. Huang, H. Furukawa, Y. Tanaka, T. Nakajima, Y. Osada and J. P. Gong, *Macromolecules*, 2007, **40**, 6658–6664.
40 Z. Lei, W. Zhu, S. Xu, J. Ding, J. Wan and P. Wu, *ACS Appl. Mater. Interfaces*, 2016, **8**, 20900–20908.
41 D. K. Roper, W. Ahn and M. Hoepfner, *J. Phys. Chem. C*, 2007, **111**, 3636–3641.
42 Q. Tian, M. Tang, Y. Sun, R. Zou, Z. Chen, M. Zhu, S. Yang, J. Wang, J. Wang and J. Hu, *Adv. Mater.*, 2011, **23**, 3542–3547.